Outflow from the ionosphere in the vicinity of the cusp

P. W. Valek,[1,2] J. D. Perez,[1] J.-M. Jahn,[3] C. J. Pollock,[3] M. P. Wüest,[3]
R. H. W. Friedel,[4] T. E. Moore,[5] and W. K. Peterson[6]

Received 29 March 2001; revised 15 November 2001; accepted 18 November 2001; published 13 August 2002.

[1] Low-energy ion outflows from the ionosphere are known to be an important source of plasma for the magnetosphere. The objective of this study is to describe the spatial relationships between low-energy ionospheric outflows and the cusp. The analysis is similar to that used in superposed epoch analyses, except that a spatial reference is used instead of a temporal one. Data from the Thermal Ion Dynamics Experiment (TIDE) supported by data from the Toroidal Imaging Mass-Angle Spectrograph (TIMAS) and Hydra, during low-altitude, perigee passes over the South Pole by the Polar spacecraft are used. The presence of isotropic ions from the magnetosheath is used to define the equatorward boundary of the cusp. By using this magnetospheric boundary as a reference point instead of invariant latitude, the temporal variability of the cusp location with respect to the Earth is removed. Poleward of this boundary in the cusp proper, observations show ionospheric outflow in addition to the isotropic magnetosheath ions. A technique used to separate the ion distributions originating from the two sources is presented and applied in order to calculate moments of the outflowing ion distribution. Ionospheric outflow is found to occur in the cleft region that extends $\approx$1.5° equatorward of the low-latitude cusp boundary and in the cusp that extends $\approx$5° poleward of this boundary. Both the parallel and perpendicular temperatures of the outflowing ions are found to be approximately a factor of 3 larger on the equatorward side of this cusp boundary, i.e., in the cleft. *INDEX TERMS:* 2736 Magnetospheric Physics: Magnetosphere/ionosphere interactions; 2724 Magnetospheric Physics: Magnetopause, cusp, and boundary layers; *KEYWORDS:* ionospheric outflow, cusp boundary

1. Introduction

[2] The ionosphere plays a significant role as a source for magnetospheric plasma [*Chappell et al.*, 1987; *Moore et al.*, 1999]. Ions of ionospheric origin have been found in such diverse regions as the ring current [*Johnson et al.*, 1977], the plasma sheet [*Peterson et al.*, 1981], and the plasma sheet boundary layer and tail lobes [*Eastman et al.*, 1984].

[3] In this paper we focus on ionospheric outflows in the cusp region. Strong outflows in the cusp have been found to be associated with an interplanetary shock and associated coronal mass ejection [*Moore et al.*, 1999], but ionospheric outflows in this region are also found to be a persistent phenomenon. See the work of *Yau and André* [1997] for a review of high-latitude outflows. *Pollock et al.* [1990], in a survey of upwelling ion events using Dynamic Explorer (DE) 1 data, found no evidence of a correlation between the probability of the occurrence of an O^+ upwelling ion event and invariant latitude. They did see, however, that the invariant latitude of where the upwelling ion events occurred was correlated with interplanetary magnetic field (IMF) B_z. They also show that the upwelling location is within the cusp poleward and equatorward boundaries as determined by the linear least squares fit as a function of IMF B_z by *Carbary and Meng* [1986]. This implies that the location of the outflow moves with the cusp. *Newell and Meng* [1992] mapped the dayside ionosphere to the magnetosphere. They reported that the most probable location of the cusp was between 11 and 13 magnetic local time (MLT) and 80° and 75° magnetic latitude. (See the work of *Smith and Lockwood* [1996] for a review of the Earth's cusp.) The temporal variability of the location of the cusp and other regions of the magnetosphere comes from its being buffeted in the solar wind [*Newell et al.*, 1989] and the tilt angle of the Earth's dipole field [*Newell and Meng*, 1989; *Zhou et al.*, 1999].

[4] The objective of this study is to understand the spatial relationship between the ionospheric plasma outflow and the location of the cusp. *Dubouloz et al.* [1998] investigated the spatial properties of the cleft ion fountain region using data from Interball Auroral Probe. They found that outflowing ions originate from a narrow (<2°) latitudinal interval just poleward of the closed field line region. In this study we observe a similar region but find that the outflow region extends further poleward into a region in

[1]Department of Physics, Auburn University, Auburn, Alabama, USA.
[2]Now at Space Science and Engineering, Southwest Research Institute, San Antonio, Texas, USA.
[3]Space Science and Engineering, Southwest Research Institute, San Antonio, Texas, USA.
[4]Los Alamos National Laboratory, Los Alamos, New Mexico, USA.
[5]Interplanetary Physics Branch, NASA Goddard Space Flight Center, Greenbelt, Maryland, USA.
[6]Laboratory for Atmospheric and Space Physics, University of Colorado, Boulder, Colorado, USA.

Copyright 2002 by the American Geophysical Union.
0148-0227/02/2001JA000107

which ions of both ionospheric and magnetosheath origin coexist.

[5] A typical pass of data is presented to show an example of the details of the structure of the cusp region of the magnetosphere. A statistical study is then performed to show the average structure of this region. We use a technique similar to superposed epoch analysis, except in a spatial reference frame instead of a temporal one. The variability of the location of the cusp is thus removed from the analysis. We identify two boundaries. One is the open-closed field line boundary. The other is associated with the appearance of isotropic ions from the magnetosheath, which corresponds to what is usually referred to as the equatorward boundary of the cusp [*Newell and Meng*, 1988]. Poleward of the cusp boundary is the region in which magnetosheath and ionospheric ions coexist. A technique to separate the ion distributions originating from the two sources is presented and applied in order to calculate moments of the outflowing ion distribution.

2. Data

[6] We use data from perigee passes of the Polar spacecraft [*Acuña et al.*, 1995] because they have several benefits over apogee passes for the purposes of this study. First, the spacecraft is much closer to the ionospheric source of the outflowing ions at its perigee, $\approx 1.8\ R_E$, than when it is at its apogee, $\approx 9\ R_E$. This means that the ions have had less time to convect away from their original ionospheric source location. This also minimizes any confusion that could be caused by the altitude dependence of the ion heating. Second, since a spatial rather than a temporal dependence is being studied, the higher spacecraft velocity at perigee will allow the spacecraft to sample the whole region before it can change appreciably. At perigee the spacecraft travels through the cusp region in the matter of a few minutes. The spacecraft takes hours to travel through the same region while at apogee.

[7] Low-energy ions are the primary species of interest in this study. The Thermal Ion Dynamics Experiment (TIDE) measures low-energy ions in an energy range from the spacecraft potential up to 450 eV. It has an angular resolution of 11.25° in the spin plane and nearly 180° perpendicular to the spin plane [*Moore et al.*, 1995]. At perigee the spacecraft potential is on the order of a volt and is negligible for this study. The spin axis is nominally perpendicular to the local magnetic field line, so TIDE can sample the whole range of pitch angles in a single spin. For the data set used here, TIDE is in a mode that integrates over all masses. The mass of H^+ is used in the calculations of the plasma moments described below. Although heavy terrestrial ions, such as O^+, do make up a significant proportion of the ionospheric outflow, H^+ is seen in abundance in all regions viewed in this study. We will show below that the resulting uncertainties in the plasma moments do not affect the conclusions drawn from the data. TIDE completes its measurements of the local plasma once each 6-s spin of the Polar spacecraft. This results in 0.1° or smaller in invariant latitude between TIDE measurement at perigee. The moments of the plasma distribution function shown below are averages in 0.1° bins.

[8] In addition to TIDE, data from the Toroidal Imaging Mass-Angle Spectrograph (TIMAS) [*Shelly et al.*, 1995] and Hydra [*Scudder et al.*, 1995] are used in this study. All three of these instruments are flown aboard Polar. TIMAS measures the plasma distribution in an energy range of 15 eV to 33 keV and provides mass identification. Hydra measures the electron spectra in an energy range from 20 eV to 20 keV.

3. Typical Pass

[9] A single perigee pass on 26 April 1997 from ≈1900 to 1915 UT is shown in Figure 1. The spacecraft is traveling from the nightside to the dayside. Data at earlier times, on the left-hand side of the plot, are the more poleward data. Figures 1a and 1b show TIMAS energy-time spectrograms of O^+ and H^+, respectively. Figures 1c and 1d show TIDE energy-time and spin angle time spectrograms. Figure 1e shows a Hydra energy-time spectrogram for the electrons. For this period of time the solar wind magnetic field was negative in both B_y and B_z. The structure shown in this plot is typical of most dayside, perigee passes near 1200 MLT, independent of IMF B_z direction.

[10] This pass can be divided into four distinct regions. Most equatorward, times later than 1908:30 UT, the plasma is on closed field lines. This region is labeled region 1 in Figure 1. The highly mobile electrons give a good determination of the location of the open-closed field line separatrix (see Figure 1e). A black line is drawn through all the panels at this time. This location is 1.12° equatorward of the boundary defined by the arrival of the magnetosheath ions used in the superposed epoch analysis below. No O^+ are seen in this region (see Figure 1a). The low-energy ions below 100 eV are dominated by a broad, rammed component (see Figure 1d). TIMAS shows a distinct band of high-energy hydrogen ions whose energy decreases at higher latitude (see Figure 1b). These are dayside plasma sheet ions.

[11] Moving poleward, region 2 is bounded by the open-closed field line separatrix equatorward and by the location of the magnetosheath ions poleward. (It should be noted that the term ''isotropy boundary'' was originally used in describing precipitation on the nightside to distinguish adiabatic and nonadiabatic regimes by *Newell et al.* [1996]). This boundary also meets the criteria used by *Newel and Meng* [1988] to define the equatorward boundary of the cusp, so region 2 is defined as the cleft. The low-energy outflow as seen in the TIDE data, the cleft fountain [*Lockwood et al.*, 1985], has an energy that is in the tens of eV range (see Figure 1c).

[12] The third region is the cusp. The equatorward boundary is determined by the analysis described in section 4. It marks the appearance of the magnetosheath ions. This boundary is indicated in Figure 1 by the vertical line at 1907:30 UT. The plasma is primarily low energy, less than 1 keV in region 3. Both region 3 and region 2 discussed in the previous paragraph show the densest plasmas. Significant amounts of O^+ are seen in the TIMAS data (Figure 1a) in only these two regions. The minimum energy of the ions then decays poleward (Figure 1b), or toward earlier times in this plot. The poleward dispersion is consistent with the velocity filter effect as described by *Rosenbauer et al.* [1975].

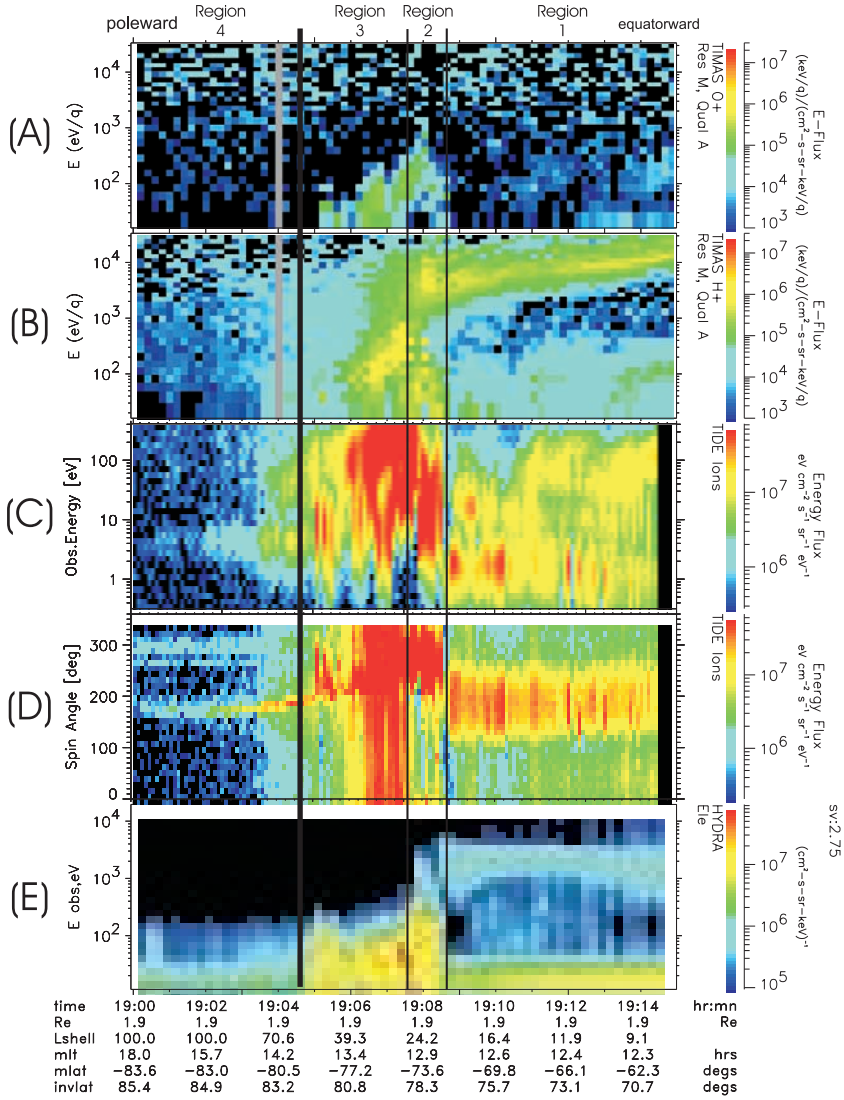

Figure 1. Plot of a dayside perigee pass from 26 April 1997: (a, b) Toroidal Imaging Mass-Angle Spectrograph (TIMAS) energy-time spectrograms for O^+ and H^+, respectively, (c, d) Thermal Ion Dynamics Experiment (TIDE) energy-time and spin-time spectrograms, and (e) Hydra electron data. The TIDE spectrograms are integrated over all masses. The TIDE spin-time spectrogram includes data from the whole of the TIDE energy range, not only from the range above 100 eV as shown in Figure 2. The vertical line at 1908:30 UT marks the open-closed field line separatrix. The magnetosheath precipitation boundary is at 1907:30 UT. The different regions indicated are discussed in the text.

[13] The fourth, most poleward region is the dayside section of the polar cap. The equatorward end of this region is less distinct than the open-closed field line separatrix boundary and the equatorward edge of the cusp. The polar cap is poleward of the location where Polar is at ≈1905 UT.

4. Superposed Epoch

4.1. Automated Cusp Identification

[14] The superposed epoch analysis performed by ordering the data by the location of the cusp. The location of the cusp was determined by finding the equatorward edge of the precipitating magnetosheath ions as observed in the TIDE data. This signature was selected since it is easily identifiable and maps the location of direct solar wind ions entry into the lower magnetosphere. It is consistent with the definition of the cusp by *Newell and Meng* [1988] as the region in which the ions have energies from ≈ 100 eV up to ≈3 keV. The particle fluxes are large and highly isotropic; that is, the flux of ions is nearly equal at all pitch angles.

[15] The interpretation is that the particles crossed the magnetopause from the magnetosheath with the expected D-shaped distribution and now have flux at all angles due to ions mirroring at various altitudes below the observation point. This high degree of isotropy in the magnetosheath distribution is caused by a large fraction of the precipitating ions mirroring below the spacecraft. The high degree of isotropy is used to find the cusp boundary. An automated technique for identifying this boundary provided for the inclusion of a large number of orbits in the analysis and

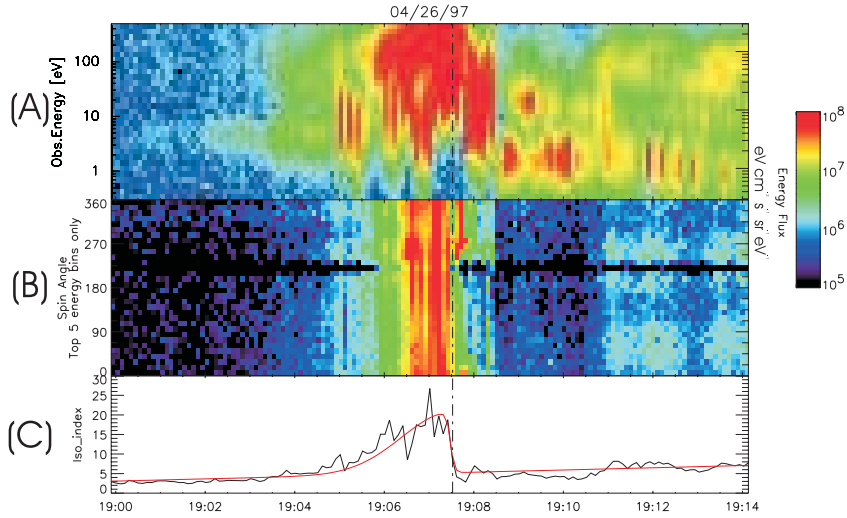

Figure 2. (a) An energy-time spectrogram of TIDE energy flux data for a perigee pass on 26 April 1997, (b) a spin angle time spectrogram using only TIDE for the energy channels above 100 eV, and (c) the calculated, black, and fitted, red, isotropy index for this period. The equatorward edge of the magnetosheath ions, cusp, is at 1907:30 UT. A vertical black line is drawn through all three panels at this time. Data from this energy range are used for the calculation of the isotropy index. The local magnetic field direction is near 300°.

removed some of the subjectivity inherent in visual inspection of data.

[16] The TIDE instrument data set is organized in a matrix of 31 logarithmically spaced energy steps and 32 equally spaced angular steps per spin. In the automated procedure the mean value of the flux and its standard deviation for a given energy step are calculated by integrating over spin angle. The dimensionless ratio of the mean of the flux to the standard deviation of the flux is defined here as the isotropy for a given energy step. As the distribution becomes more isotropic, the standard deviation of the flux goes to zero, making the isotropy large.

[17] Periods with low flux may appear isotropic but will not have a large isotropy value. The inherent noise in a microchannel plate (MCP) based detector system, like the one used in TIDE, will have a standard deviation of the flux on the order of the square root of the flux. This will keep the value of the isotropy low for cases of low flux. The term isotropy index, defined as

$$\text{isotropy index} = \sum_{E>100\,\text{eV}} \frac{\text{mean(flux)}}{\text{standard deviation(flux)}}, \qquad (1)$$

is the value of the isotropy summed over the five highest energy bands of TIDE. The five highest energy bands are those above 100 eV and are in the energy range of the magnetosheath ions.

[18] A single perigee pass from 26 April 1997 is shown in Figure 2 to illustrate the boundary identification technique. This is the same time period shown in Figure 1. Figure 2a shows an energy-time spectrogram of energy flux. This is an expanded version of Figure 1c. The most equatorward extent of the magnetosheath ions is at 1907:30 UT. Figure 2b shows a spin angle time spectrogram. Data for this spectrogram only include the energy covered by TIDE that contributes to the isotropy index, i.e., the five highest bands of TIDE covering energies above 100 eV. It is therefore different than Figure 1d because it does not contain the spin angle data that correspond to the intense low-energy flux between 1907:30 and 1908:30 UT. The high flux and high isotropy can be seen between ≈1905 and 1907:30 UT. Figure 2c shows the isotropy index for this pass (black line). Note how the isotropy index has a gradual slope on the poleward side and a more abrupt, step-like profile on the equatorward side. This is consistent with previous findings, for example, those of *Newell and Meng* [1988], that showed a sharp equatorward boundary to the cusp and a more diffuse poleward boundary.

[19] The isotropy index is empirically fit by the function

$$F(t) = A + Bt + Ct^2 + D\exp\left[-\frac{1}{2}\left(\frac{t-t_0}{\Delta_0}\right)^2\right] \cdot \left\{\frac{1}{2}\left[1-\tanh\left(\frac{t-t_1}{\Delta_1}\right)\right]\right\} \qquad (2)$$

for passes where increasing times, t, indicate decreasing latitudes. The terms A, B, and C are fitting parameters to fit the background to a second-order polynomial, and D is the amplitude of the isotropy index at the cusp region. The centroid and the width of the cusp region are described by t_0 and Δ_0, and the centroid and ramp width of the boundary are described by t_1 and Δ_1. The hyperbolic tangent term gives step-like behavior as Δ_1 becomes small. The fit to the data by $F(t)$ is shown in Figure 2c (red line).

[20] The location of the equatorward edge of the cusp is defined at the value of t for which

$$\frac{1}{2}\left[1-\tanh\left(\frac{t-t_1}{\Delta_1}\right)\right] = 0.25 \qquad (3)$$

and is termed the isotropy boundary or the equatorward boundary of the cusp in this paper. The value of 0.25 was

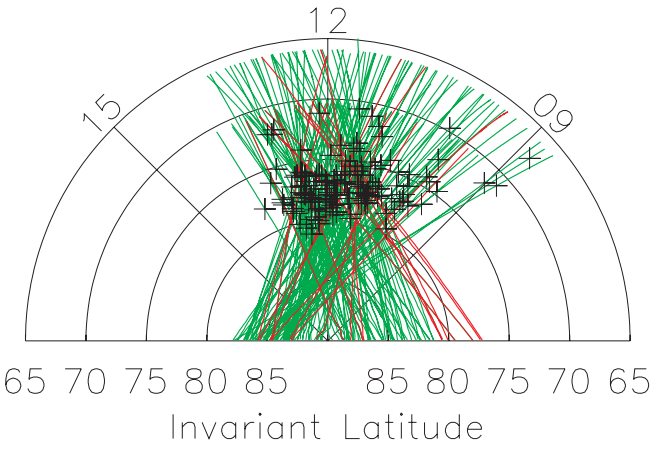

Figure 3. Plotted are the orbital paths of the Polar spacecraft for the data set used. The paths are plotted as a function of invariant latitude and magnetic local time. The green traces show passes where a cusp boundary is successfully found. Location of the cusp boundary is shown by the crosses. The red traces are passes where a cusp boundary is not found.

chosen after inspecting a series of test cases. The vertical line through all three panels in Figure 2 shows the location of the cusp's equatorward boundary. When this technique is applied to all the data used in this study, the mean location of the equatorward boundary of the cusp is at 76.85° of invariant latitude with a standard deviation of 2.09°.

4.2. Results for all Events

[21] The cusp boundary location is used to perform a superposed epoch analysis. Only passes where the spacecraft has at least one spin of data in a region bounded by 1100 to 1300 MLT and from −85° to −70° of magnetic latitude over the Southern Hemisphere are included. Within these boundaries the cusp can be found with a high probability [*Newell and Meng*, 1992]. Orbits that pass through this bounded region but have the determination of the cusp boundary outside these limits are still included in this study.

[22] The Polar spacecraft orbit meets the above requirements for 187 perigee passes. When times are removed during which TIDE is turned off for reasons such as spacecraft maneuvers, the total number of acceptable passes becomes 160. The automated code was able to identify the cusp in the data 141 times, or ≈88 of the passes with TIDE on. Figure 3 shows the paths of Polar for the data set used here as a function of MLT and invariant latitude. The determined cusp boundaries for this data set are shown with crosses. The green traces are for the passes where a cusp boundary is successfully identified. The red traces show the paths of Polar for the 19 passes when a cusp boundary was not identified.

[23] Passes where a cusp boundary was not identified are distributed through the region considered in this analysis. This shows that the passes with no cusp identification have no bias in the orbit path. The IMF for these passes was inspected to see if that was a source of a bias. All but one of the 19 passes without a cusp have the values of the IMF distributed evenly in the positive and negative bins. The one case that stands out is from 6 April 2000. A major storm occurs at this time. The reason that the cusp was not identified was that it was pushed too far equatorward to be seen by TIDE, because the cusp signature is within the region where TIDE is shutdown for the radiation belts. Finding the cusp boundary is not due to a bias in sampling.

[24] The average of the plasma moments from the TIDE data with an identifiable cusp signature is shown in Figure 4. Plotted as a function of invariant latitude are, from the top, parallel velocity in km s^{-1}, parallel and perpendicular temperature in eV, and ion density in cm^{-3}. Since the data come from perigee passes over the Southern Hemisphere, a positive parallel velocity implies outflow, so a net outflow is seen on average for all invariant latitudes above 73°. The net inflow at lower latitude is a result of the flux at ≈100 eV (see Figure 1c) and at spin angles below 100° (see Figure 1d). As shown in Figure 3, the location of the cusp varies over ≈5°

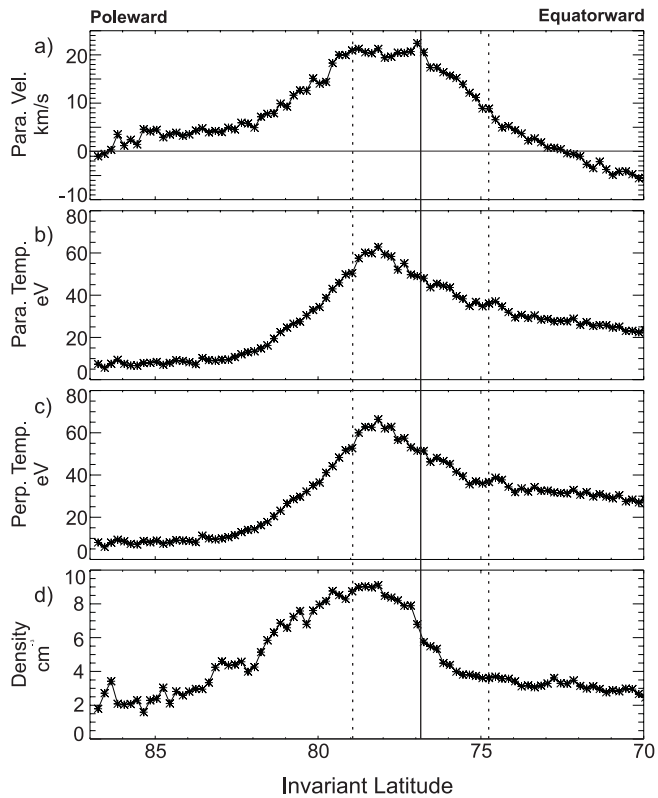

Figure 4. Average plasma moments plotted as a function of invariant latitude as measured by TIDE: (a) parallel velocity in km s^{-1}, (b, c) parallel and perpendicular temperatures in eV, and (d) density. The data set used for the average comes from perigee passes from the months of March, April, and May from the years of 1997, 1998, 1999, and 2000, where the orbit travels between 1100 and 1300 MLT. In Figure 4a, perigee passes are over the Southern Hemisphere, so positive parallel velocities indicate outflow. The TIDE for this data set is integrated over all masses, so a mass equal to H^+ is assumed to calculate the moments. The solid vertical line through the panels indicates the mean location of the equatorward boundary of the cusp as described in the text. The dashed lines are drawn one standard deviation away from the mean location of the equatorward boundary of the cusp.

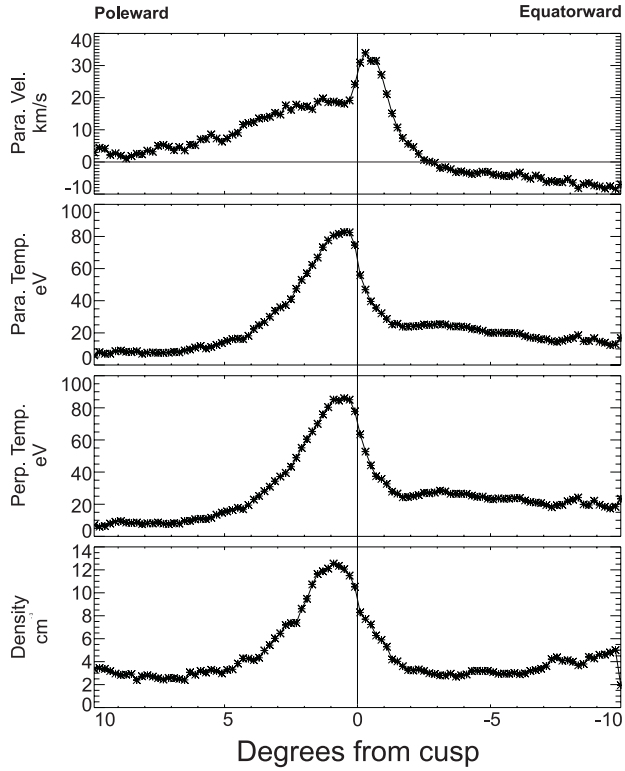

Figure 5. Average plasma moments plotted as a function of distance from the magnetosheath precipitation boundary as measured by TIDE. Format of this plot is the same as in Figure 4.

of latitude for these events. This motion will obscure any spatial structures smaller than 5° in the observed moments.

[25] A superposed epoch analysis is performed on the data set using the technique described above to find the equatorward boundary of the cusp for each perigee pass. Figure 5 shows the effect that this sorting has on the plasma moments. The format of Figure 5 is the same as that in Figure 4, except the data are plotted as a function of degrees of invariant latitude from the equatorward edge of the isotropy boundary, not as a function of invariant latitude. Comparing Figure 5 to Figure 4 shows that sharper structure emerges after the superposed epoch analysis is performed. For the full set of events used in this analysis the error estimates of the average moments are small. In analysis shown below in which the events are separated into groups with the IMF $B_z <$ and > 0, the estimated uncertainties become larger. The estimated uncertainties are then around 15% or smaller.

[26] As mentioned above, an ion species of H^+ is used in the calculations of the TIDE moments. TIDE measures differential directional energy flux. To calculate the bulk temperature of the plasma distribution, no further information is required. The temperature moments shown here are therefore not affected by the assumption that the species measured consists on only H^+. In the calculation of the density from the measured differential directional energy flux, the density scales as the $\sqrt{m}$, where the dimensionless m is the species mass. The densities shown here are then a lower bound of the actual density. The calculation of the velocity from the measured differential directional energy flux scales as $\frac{1}{\sqrt{m}}$. In regions with significant O^+ the velocity shown here is an upper bound on the actual parallel velocity.

[27] It should be noted that the TIMAS data for the 26 April 1997 pass show O^+ densities between the times of 1905:00 and 1908:30 UT that are ≈10–20% of the H^+ densities. Also, *Pollock et al.* [1990] found using the Retarding Ion Mass Spectrometer (RIMS) data from Dynamics Explorer (DE) 1 spacecraft that O^+ is a significant fraction of the composition of the upwelling [*Moore et al.*, 1986] ion events they studied.

[28] To estimate the error from using only H^+, we make the simplifying assumption that when two species are present, hydrogen and another mass m, they are not separated in energy. The density from the two species is then $(x + \sqrt{m}(1 - x))$ times the density calculated using the hydrogen alone. Here x is the percent of hydrogen. For the case of 20% O^+ (x = 0.8), the actual density measurement will be 1.6 times larger than that shown. For two species the velocity will be $(x + 1\sqrt{m}(1 - x))$ times the value shown. Again for 20% O^+, the actual velocity will be 0.85 of the value shown.

[29] For each of the moments shown in Figure 5 the character of the plasma changes ≈1.5° equatorward of the boundary. As we move toward the boundary, the parallel velocity shows a dramatic increase in the outflow velocity to nearly 35 km s^{-1}. Temperature and density show increases as well. Immediately poleward of the boundary, the parallel velocity abruptly drops to near half of its peak value. The parallel and perpendicular temperature and density all peak poleward of the boundary.

[30] The behavior of the moments around the boundary can be explained by the fact that TIDE is measuring a combination of the low-energy outflowing ions and the precipitating magnetosheath ions. Figure 6a shows a phase space density (PSD) plot for a region with only the ionospheric ions and Figure 6b shows the same for a region with both the ionospheric ions and magnetosheath ions. The PSD plots cover two, 6-s spins of data from the 26 April 1997 perigee pass shown in Figures 1 and 2. Both Figures 6a and 6b have the local magnetic field direction pointing up. The crosses plotted in these panels each represent the stationary point in three different frames of reference. The first is in the Earth frame and is the white cross in the center of the panels. The second is in the spacecraft frame of reference and is the thin black cross located in the center of the TIDE data. The third is the thick black cross located at the calculated plasma velocity.

[31] Figure 6a shows data from 1907:43 UT, slightly equatorward of the isotropy boundary, i.e., in the cleft region. Ionospheric outflow is clearly seen here, with a calculated parallel velocity of 30 km s^{-1}. There is very low phase space density in the anti-field-aligned direction. Figure 6b is from 1907:13 UT, slightly poleward of the boundary, i.e., in the cusp. Here the ionospheric outflow is still clearly seen, but it is now immersed in the isotropic magnetosheath distribution. The calculated plasma velocity shown in Figure 6b is at 15 km s^{-1}. As described in the discussion of Figure 5, effects of the magnetosheath ions can be seen in the other moments as well. The sharp increase in the parallel and perpendicular temperature poleward of the boundary is caused by hot magnetosheath ions. The magnetosheath distribution also contributes to the

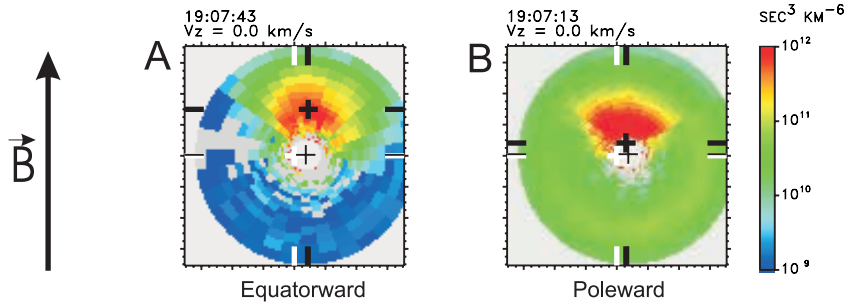

Figure 6. Single spins of TIDE data displayed in phase space density (PSD) plots for (a) a spin equatorward of the magnetosheath precipitation boundary and (b) a spin poleward of the magnetosheath precipitation boundary. Each panel is in the spin plane, with the local magnetic field pointing up. The small gray region in the center of the plot and the larger gray region on the outside of the plot show phase space not measured. The white cross in the center of the panels shows the Earth's reference frame, the thin black cross shows the spacecraft reference frame, and the thick black cross shows the calculated plasma velocity.

density poleward of the boundary. Including both the ionosphere outflowing ions and the precipitating magnetosheath ions in the moments calculation clearly skews the results poleward of the boundary.

[32] To better characterize the low-energy ion outflows, the magnetosheath distribution needs to be separated and removed from the data from which the moments are calculated. Each of the distributions in Figure 6 consist of 32 spin angle steps and 31 energy steps. A series of one-dimensional fits over energy were performed for each of the 32 spin angle steps of each 6-s spin. After the fits are performed, these 32 slices of the data can be reassembled to recreate an empirical model of the flux for that spin. Performing the series of one-dimensional fits has the advantage that it does not require an assumed functional form to be imposed on the second dimension of the data, here the spin angle. For each spin angle the energy flux as a function of energy is fitted to each of

$$M(E) = A_0(E - A_1)^2 \exp\left[-\frac{E - A_1}{A_2}\right], E > A_1 = 0, E \le A_1 \quad (4)$$

$$I(E) = B_0 \exp\left[-\frac{1}{2}\left(\frac{\ln(E) - B_1}{B_2}\right)^2\right] + B_3 \quad (5)$$

$$B(E) = M(E) + I(E) \quad (6)$$

with E as the measured energy and the terms A_n and B_n being fitting parameters. $M(E)$ fits the magnetosheath distribution, $I(E)$ fits the ionospheric distribution, and $B(E)$ is the compound fit of both magnetosheath and ionospheric distributions. The form of equation (4) is that of a Maxwellian in units of energy flux. The form of equation (5) is an empirical fit and has no physical interpretation. The best fit is determined by the value of χ^2. The two-distribution fit must be significantly better than the one distribution fits to be chosen; that is, we impose that the ratio of the χ^2 of the two-distribution fit to the χ^2s of either of the one-distribution fits must be lower than 0.7.

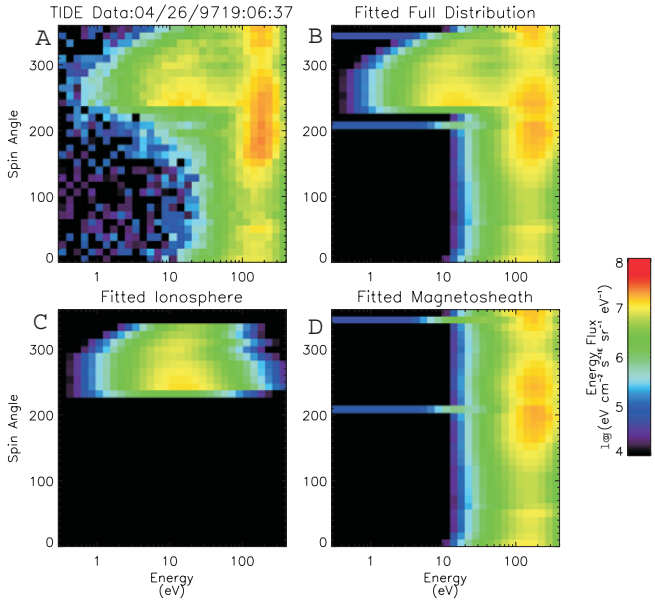

Figure 7. One spin of data from 1906:37 UT, poleward of the magnetosheath precipitation boundary: (a) actual energy flux as measured by TIDE, (b) fitted data to the empirical model in equations (4), (5), and (6), and (c, d) ionospheric and magnetosheath distributions separated from the fitted data, respectively. In each panel, measured or fitted energy flux is plotted as a function of energy and spin angle. The local magnetic field direction is at the spin angle of 300°.

[33] Figure 7 shows the results of such a fitting one spin of data from 1906:37 UT, that is, poleward of the boundary. In each panel, measured or fitted energy flux is plotted as a function of energy and spin angle. The local magnetic field direction is at the spin angle of 300°. Figure 7a shows the energy flux measured by TIDE. The magnetosheath ions shown in Figure 7d are seen at all angles above 90 eV. The outflowing ionosphere ions shown in Figure 7c are seen between angles of 225° and 360° in the energy range of around 10–90 eV. Figure 7b shows the results of the fit. The empirical fit of the data has good agreement with the measured data.

[34] This technique of fitting multiple distributions to the data fails when the energy of the two distributions overlaps significantly. This happens most often near the equatorward

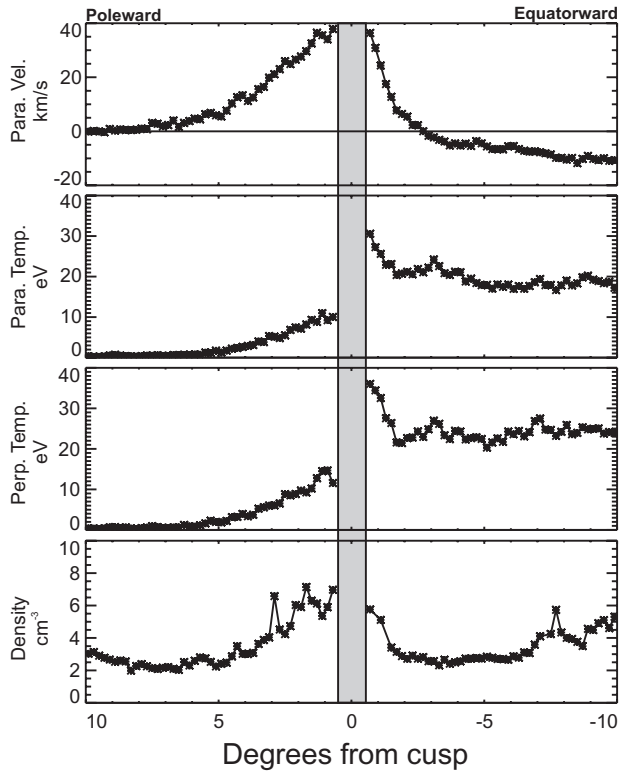

Figure 8. Plots of the average plasma moments as calculated from the fitted ionosphere. These moments are plotted as a function of distance from the magnetosheath precipitation boundary as measured by TIDE. Format of this plot is the same as that in Figures 4 and 5. The gray bar through the panels ±0.5° the magnetosheath precipitation boundary indicates the region of poor confidence in the ionospheric fitting procedure.

edge of the cusp, the magnetosheath ion isotropy boundary. Because of this, data within ±0.5° of the isotropy boundary will be ignored in the final calculation of the plasma moments.

[35] Figure 8 shows the plasma moments calculated from the fitted ionospheric ions only. The order of the panels is the same as that in Figures 4 and 5. The vertical gray bar through the panels indicates the region of poor confidence in the separation technique described above. The fitted parallel velocity data do not show the drop in velocity as seen when the magnetosheath ions are included in the moments. This is expected since the drop in velocity poleward of the boundary is from the inclusion of the precipitating magnetosheath ions. The parallel and perpendicular temperatures both show significant heating equatorward of the cusp boundary. The outflowing ions poleward of the boundary are significantly colder than the equatorward ions. Exclusion of the magnetosheath ions does not change the observation that the ionospheric plasma shows heating and outflow 1.5° equatorward of the low-latitude cusp boundary.

[36] Visual inspection of the Hydra electron data for all the 1997 passes used in this study shows that the open field line separatrix is, on average, 1.3° equatorward of the magnetosheath boundary, with a standard deviation of 0.8°. This is essentially the same as the location of the change in character of the ion moments 1.5° equatorward of the magnetosheath ion boundary as shown in Figures 5 and 8. This suggests that the electrons, or processes associated with them, are more important to the energization of ionospheric outflows than the magnetosheath ions. This is in agreement with *Canton et al.* [1996], who showed results suggesting that the effects of soft electron precipitation and downward magnetospheric electron heat fluxes can account, in general, for the features of the ionospheric outflows.

[37] The statistical results presented above made no reference to the state of the IMF during the measurements. To investigate the effect that IMF B_z has on the structure of the outflows, the data set was separated into cases with B_z southward and B_z northward. Data from the Wind spacecraft are used to determine the value of B_z. The Wind data set was shifted in time to account for the travel time of the solar wind from Wind to the Earth's magnetosphere. Only passes where the sign of B_z in the time-shifted data set did not change for more than 30 min prior to the time where Polar crossed the isotropy boundary where included.

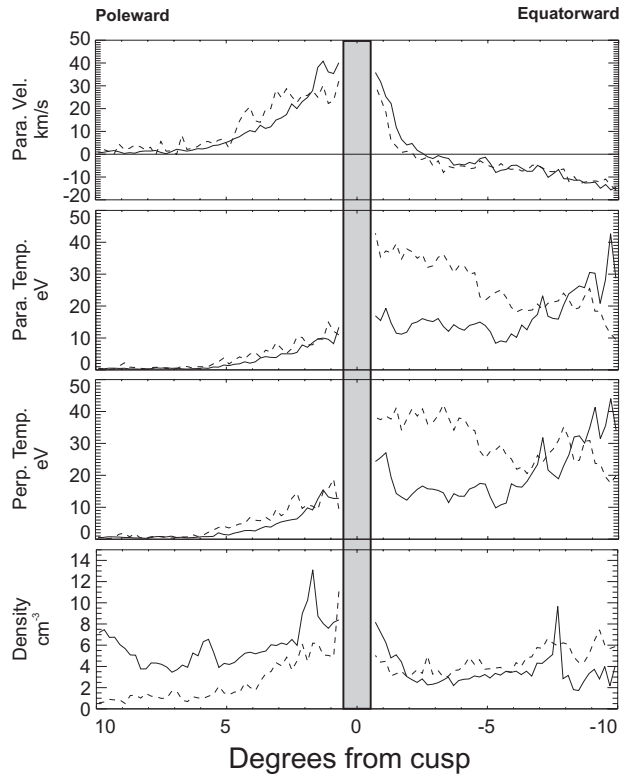

Figure 9. IMF B_z effect on average plasma moments as calculated from the fitted ionosphere. Solid line shows the moments for B_z southward, and the dashed line is for B_z northward. IMF was determined with data from the Wind spacecraft. This plot is the same format as that in Figures 4, 5, and 8. The gray bar through the panels ±0.5° the magnetosheath precipitation boundary indicates the region of poor confidence in the ionospheric fitting procedure.

[38] When the data are separated by IMF B_z, 33 passes have a southward B_z and 31 passes have a northward B_z. Figure 9 shows the moments for the fitted ionosphere with the solid line for the B_z south case and the dashed line for the B_z north case. The format of Figure 9 is the same as Figure 8. Uncertainties in Figure 9 are on the order of ±5 km s^{-1} in the parallel velocity, ±5 eV for the temperatures, and ±1 cm^3 for the density.

[39] The sharp equatorward boundary of the cusp remains a distinct feature regardless of the value of B_z. The main features of the ionospheric outflow do not show a strong dependence on B_z. The parallel velocity for northward B_z does have a somewhat smaller outflow velocity in the region of the cusp boundary, and the peak value for $B_z > 0$ extends farther poleward of the boundary before both cases drop to zero at approximately the same latitude with respect to the cusp boundary. The bulk outflow for both signs of B_z still has a dramatic increase 1.5° of the cusp boundary. The parallel and perpendicular temperatures still decrease sharply poleward of the cusp boundary, but for northward B_z there seems to be greater heating of the ionospheric outflow in the cleft region. For $B_z > 0$ the higher temperatures persist equatorward of the cleft where density and outflow velocity are low. The density of the ionospheric outflow is higher for northward B_z in the cusp region and even further poleward.

5. Summary

[40] A statistical study of the spatial dependence of the low-energy ion outflow in the magnetospheric cusp region has been performed. The data set used in this study consisted of perigee passes of the Polar spacecraft between 1100 and 1300 MLT, in the spring months of 1997–2000. Regular, persistent features of the ionospheric outflow were found by referring the moments of the plasma distribution to the equatorward boundary of the cusp. The cusp boundary was identified by the presence of isotropic magnetosheath plasma. A technique to separate the plasma of ionospheric origin from the magnetosheath plasma was demonstrated. Thus plasma moments were calculated using only the distribution function of the ionosphere ion. The outflow begins in the cleft ≈1.5° equatorward of the cusp boundary at a point that coincides with the open-closed field line boundary. It peaks at the cusp boundary and extends another 4–5° poleward of the cusp boundary in the cusp. The parallel and perpendicular temperatures peak at the cusp boundary and then drop precipitously poleward of this boundary.

[41] The effect of IMF on the moments was investigated by separating the data into the passes with B_z positive and negative. The sharp cusp boundary remained a distinct feature independent of the sign of B_z. Poleward of this boundary, magnetosheath plasma was observed, and equatorward in the cleft region only ionospheric plasma was found. The most dramatic dependence on the sign of B_z was the greater heating of ionospheric outflow in the cleft region for B_z positive.

[42] **Acknowledgments.** We would like to thank R. Lepping of NASA/GSFC and CDAWeb for providing the Wind MFI data.

[43] Janet G. Luhmann thanks Harald U. Frey and Dominique C. Delcourt for their assistance in evaluating this paper.

References

Acuña, M. H., K. W. Ogilvie, D. N. Baker, S. A. Curtis, D. H. Fairfield, and W. H. Mish, The global geospace program and its investigations, *Space Sci. Rev.*, *71*, 5–21, 1995.

Canton, R., J. L. Horwitz, P. G. Richards, and C. Liu, Modeling of *F*-region ionospheric upflows observed by EISCAT, *Geophys. Res. Lett.*, *23*, 1537–1540, 1996.

Carbary, J. F., and C.-I. Meng, Correlation of cusp latitude with B_z and *AE*(12) using nearly one year's data, *J. Geophys. Res.*, *91*, 10,047–10,054, 1986.

Chappell, C. R., T. E. Moore, and J. H. Waite Jr., The ionosphere as a fully adequate source of plasma for the Earth's magnetosphere, *J. Geophys. Res.*, *92*, 5896–5910, 1987.

Dubouloz, N., D. Delcourt, M. Malingre, J.-J. Berthelier, and D. Chugunin, Remote analysis of cleft ion acceleration using thermal plasma measurements from Interball Auroral Probe, *Geophys. Res. Lett.*, *25*, 2925–2928, 1998.

Eastman, T. E., L. A. Frank, W. K. Peterson, and W. Lennartsson, The plasma sheet boundary layer, *J. Geophys. Res.*, *89*, 1553–1572, 1984.

Johnson, R. G., R. D Sharp, and E. G. Shelly, Observations of ions of ionospheric origin in the storm-time ring current, *Geophys. Res. Lett.*, *4*, 403–406, 1977.

Lockwood, M., M. O. Chandler, J. L. Horwitz, J. H. Waite Jr., T. E. Moore, and C. R. Chappel, The cleft ion fountain, *J. Geophys. Res.*, *90*, 9736–9748, 1985.

Moore, T. E., M. Lockwood, M. O. Chandler, J. H. Waite Jr., A. Persoon, and M. Sugiura, Upwelling O^+ ion source characteristics, *J. Geophys. Res.*, *91*, 7019–7031, 1986.

Moore, T. E., et al., The Thermal Ion Dynamics Experiment and Plasma Source Instrument, *Space Sci. Rev.*, *71*, 409–458, 1995.

Moore, T. E., et al., Ionospheric mass ejection in response to a CME, *Geophys. Res. Lett.*, *26*, 2339–2342, 1999.

Newell, P. T., and C.-I. Meng, The cusp and the cleft/boundary layer: Low altitude identification and statistical local time variation, *J. Geophys. Res.*, *93*, 14,549–14,556, 1988.

Newell, P. T., and C.-I. Meng, Dipole tilt angle effects on the latitude of the cusp and cleft/low-latitude boundary layer, *J. Geophys. Res.*, *94*, 6949–6953, 1989.

Newell, P. T., and C.-I. Meng, Mapping the dayside ionosphere to the magnetosphere according to particle precipitation characteristics, *Geophys. Res. Lett.*, *19*, 609–612, 1992.

Newell, P. T., C.-I. Meng, D. G. Siebeck, and R. Lepping, Some low-altitude cusp dependencies on the interplanetary magnetic field, *J. Geophys. Res.*, *94*, 8921–8927, 1989.

Newell, P. T., Y. I. Feldstein, Y. I. Galperin, and C.-I. Meng, Morphology of nightside precipitation, *J. Geophys. Res.*, *101*, 10,737–10,748, 1996.

Peterson, W. K., R. D. Sharp, E. G. Shelly, R. G. Johnson, and H. Balsiger, Energetic ion composition of the plasma sheet, *J. Geophys. Res.*, *86*, 761–767, 1981.

Pollock, C. J., M. O. Chandler, T. E. Moore, J. H. Waite Jr., C. R. Chappell, and D. A. Gurnett, A survey of upwelling ion event characteristics, *J. Geophys. Res.*, *93*, 18,969–18,980, 1990.

Rosenbauer, R. G., H. Gruenwaldt, M. D. Montgomery, G. Paschmann, and N. Skopke, Heos 2 plasma observations in the distant polar magnetosphere: The plasma mantle, *J. Geophys. Res.*, *80*, 2723–2737, 1975.

Scudder, J., et al., Hydra: A 3-dimensional electron and ion hot plasma instrument for the Polar spacecraft of the GGS mission, *Space Sci. Rev.*, *71*, 459–495, 1995.

Shelly, E. G., et al., The Toroidal Imaging Mass-Angle Spectrograph (TIMAS) for the Polar mission, *Space Sci. Rev.*, *71*, 497–530, 1995.

Smith, M. F., and M. Lockwood, Earth's magnetospheric cusps, *Rev. Geophys.*, *34*, 233–260, 1996.

Yau, A. W., and M. André, Sources of ion outflow in the high latitude ionosphere, *Space Sci. Rev.*, *80*, 1–25, 1997.

Zhou, X.-W., C. T. Russell, G. Le, S. A. Fuselier, and J. D. Scudder, The polar cusp location and its dependence on dipole tilt, *Geophys. Res. Lett.*, *26*, 429–432, 1999.

R. H. W. Friedel, Los Alamos National Laboratory, Los Alamos, NM 87545, USA.

J.-M. Jahn, C. J. Pollock, and M. P. Wüest, Space Science and Engineering, Southwest Research Institute, San Antonio, TX 78228, USA.

T. E. Moore, Interplanetary Physics Branch, NASA Goddard Space Flight Center, Greenbelt, MD 20771, USA.

J. D. Perez and P. W. Valek, Department of Physics, Auburn University, Auburn, AL 36849, USA. (pvalek@swri.edu)

W. K. Peterson, LASP, University of Colorado, Boulder, CO 80303, USA.